

Thermal and Structural Analysis of Nd³⁺ Doped Y₂O₃- SiO₂ Nanopowder

Rachna Ahlawat

Assistant Professor, Department of Physics,
Ch. Devi Lal University, Sirsa, Haryana (India)

ABSTRACT

Synthesis of Nd doped Y₂O₃:SiO₂ nanopowder around moderate temperature has been carried out using sol gel technique. Moreover, monitoring of shape, size, crystallinity and densification of the prepared powder samples were also demonstrated using well known characterization techniques. The X-ray diffraction technique was used for phase identification, structural analysis, and grain size determination. FTIR spectra of the prepared powder were taken at room temperature in the range 400-4000 cm⁻¹. These spectra provide valuable information about the phase composition as well as bonding in the annealed composites. The morphology of nanoparticles and particle size was confirmed by Transmission Electron Microscope. The present work is of basic importance for better understanding of the mechanisms of photonic devices, catalytic systems, including lasers, opto-and micro-electronics, sensors and optical fiber amplifiers etc.

Keywords: Sol-gel, Yttrium Oxide, XRD, FTIR, TEM.

I. INTRODUCTION

Cubic Y₂O₃ is a potentially useful material for doping with lanthanide ions in laser applications because of excellent properties such as high melting temperature of over 2673K, good chemical stability, low phonon energy, high thermal conductivity, etc [1-2]. As a well known phosphors host material, yttria has been used in cathode radiation tube (CRT), field emission display (FED), and thin film electroluminescence (TFEL) devices [3-5]. From last decade, as a result of its high corrosion resistance, thermal stability and transparency over a wide wavelength region from violet to infrared light, research focus is deviated towards composite of yttria polycrystalline powder with different oxide like ZrO₂, HfO₂ and recently with SiO₂ [6-8]. The majority of the work, which has been reported in the literature, deals with the luminescent trivalent lanthanide ions Ln³⁺, in a free- standing form. It would be interesting to investigate the structural and optical behavior of Nd-doped Y₂O₃ nanocrystals dispersed in transparent medium such as SiO₂ glass, which can stabilize and protect the nanoparticles. One of the another major advantages of Nd doped Y₂O₃-SiO₂ laser host materials is their ability to be easily drawn into flexible optical fibers for various photonic applications, e.g., laser systems, optical fibre amplifier and integrated waveguide [9-12]. Sol-gel has the advantages of simple experimental procedure, relatively low reaction temperature, and short reaction time with low cost [13-14]. Powders obtained by this method also have fine grain size, narrow size distribution, and homogeneously doped Nd³⁺ ion. There is increasing recognition that sol-gel synthesis offers growth control capabilities that can be conveniently exploited in preparing these desirable fine particles. In this regard, the effort is focused on the preparation of highly dense

$\text{Nd}^{3+}:\text{Y}_2\text{O}_3\text{-SiO}_2$ powder and investigated the effect of low calcination temperature on the morphology and densification of the powder.



II. EXPERIMENTAL

2.1 Sample preparation

For sol-gel synthesis, high purity reagents: Tetraethoxysilane (Aldrich 99.99%), ethanol (Merck 99.9%) and double distilled water were mixed in the presence of hydrochloric acid as catalyst. To prepare the samples molar ratio of the starting solution was taken as 1:0.5:0.3:0.03 for $\text{H}_2\text{O}:\text{C}_2\text{H}_5\text{OH}:\text{HCl}:\text{TEOS}$. In order to have Nd doped Y_2O_3 powder, 3.5 wt % of neodymium salt was introduced in appropriate amount of yttrium oxide separately in the pre-hydrolyzed solution under heating. The prepared composition was further stirred for 3.5 h, so that it became a dense sol and finally a gel formation. This gel was kept at room temperature for 21 days for aging of the samples. After aging, the samples were further dried at 110°C for 30 hours in air oven and then dried samples were powdered by pestal-motrar.

2.2 Characterizations

The x-ray diffractograms were taken with the help of XPERT-PRO x-ray diffractometer operated at 45 kV and 40 mA, using monochromatic Cu $K\alpha$ radiation of wavelength 1.5406 \AA in the different 2° ranges. FTIR spectra of the nanocomposites (as-prepared and annealed samples) were taken at room temperature using perkin Elmer 400 spectrophotometer in the range $400\text{-}4000 \text{ cm}^{-1}$. The morphology of various samples was studied and particle size was confirmed by Transmission Electron Microscope (Hitachi 4500 micrograph).

III. RESULT AND DISCUSSION

3.1 Thermal Analysis

The DTA and thermo-gravimetric (TG) measurements were conducted, using a Simultaneous Thermal Analyzer (STA) apparatus, on the neodymium doped sol-gel powder obtained by drying the precursor gel at 110°C . The DTA and TG thermograms were recorded for sample S1 at a scan rate of $5^\circ\text{C}/\text{min}$ in air flux. This study allows forecasting the crystallization temperature of the material. Differential thermal analysis (DTA) and thermo-gravimetric analysis (TG) were used to identify the most favorable conditions for thermal decomposition of the gel precursor or by calcinations, which makes it possible to obtain a fully reacted powder with desired phase and chemical composition and a fine- structure which is maintained under a variety of conditions.

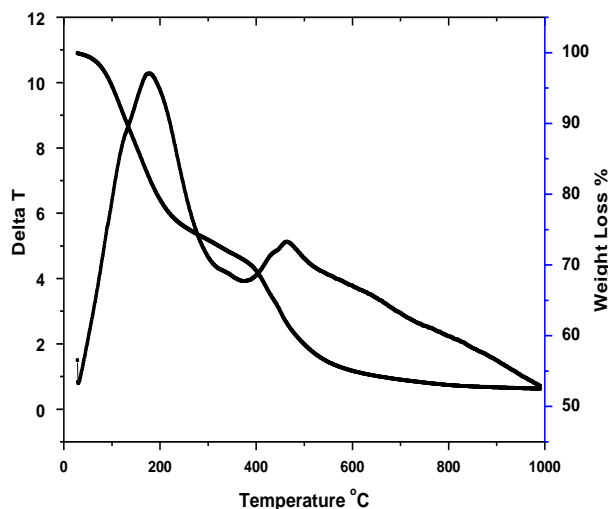


Figure 3.1: DTA- TGA curve for as prepared sample S1.

The TG curve as shown in the Fig. 3.1 is indicative of multistep decomposition behavior during thermal treatment of the precursor gel. A small weight loss from 40-120°C is due to the loss of physically adsorbed water. A large weight loss from 170°C - 470°C accompanied by two exothermic peaks centered at about 178°C-463°C is attributed to the decomposition and combustion of precursor. Most of the weight loss occurs below 600°C and the total weight loss over this range is 48 %. Small hump at 370 °C indicates Endothermic peak observed in the DTA curve which arises due to oxidation of organic compounds. No evident weight loss at temperatures >600°C indicates completion of the thermal decomposition of the precursor and indicate the crystallization of the prepared nanopowder. TG curves for the as prepared sample obtained by using the TEOS gel process.

3.2 X-Ray Diffraction (XRD) Analysis

X-ray diffraction technique can be used for phase identification, structural analysis, and grain size determination. XRD pattern for sample S1 has been shown in Fig. 3.2. The diffraction pattern of as-prepared sample depicts a very strong and sharp diffraction line centered at $2\theta \sim 25.65^\circ$ and a series of weak peaks between 10° to 45° . The sharp lines could be ascribed by characteristic diffraction of silicon oxide hydrate (JCPDS card no. 82-1179) and weak peaks between 10° to 20° may be assigned to yttrium nitrate hydrate (JCPDS card no. 84-2195) respectively [5]. These sharp lines of dried sample signify bulk behavior of hydrous precursor's nuclei and they are also suggesting that the precursors have not decomposed. In general, annealing at low temperature decomposes the precursor, initiates interfacial reaction between solids and eliminates impurities/pores associated with grain growth.

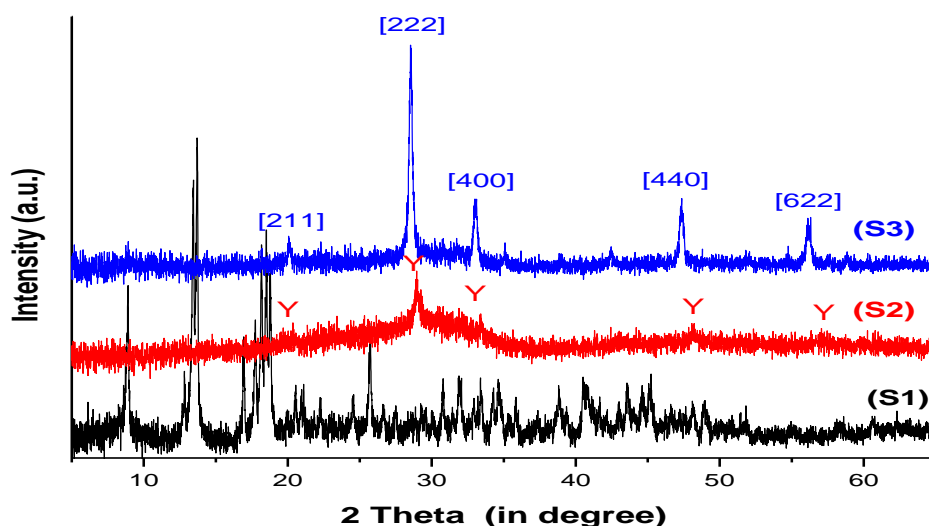


Figure 3.2: The XRD pattern of sample S1, S2 and S3.

The XRD pattern of annealed at 450°C sample S2 reveals that the characteristic peak of silicon oxide hydrate precursor has vanished completely which implies that this precursor has been decomposed and interfacial interaction has also begun in the sample. Due to this fact, a strong but slightly broad new peak appeared at $2\theta \sim 28.52^\circ$ with some weak new peaks at $2\theta \sim 20.01^\circ$, 33.11° , 47.39° and 56.12° in the diffraction pattern. The occurrence of these new peaks infers development of a new crystalline phase in the sample. Furthermore, the sample was annealed up to 850°C to examine the effect of temperature on structure of the prepared crystalline powder. In sample S3, different diffraction peaks are appeared at $2\theta \sim 20.12^\circ$, 28.92° , 33.47° , 48.22° and 57.97° . A significant increase in intensity and sharpness of the characteristic peaks of Y_2O_3 in sample S3 confirms the increase in its crystallinity and size. The crystalline phase for sample S2 and S3 was calculated from the observed X-ray diffractograms using the check cell programme and JCPDS (Joint Committee Pattern Diffraction Studies) data. In order to identify structure of the polycrystalline powder, phase corresponding to diffraction peaks at different angles in samples S2 and S3 could be assigned to cubic Y_2O_3 structure by comparing the obtained data with the JCPDS card no. 41-1105 and space group $Ia\bar{3} (T_h^7)$ [16]. In order to identify structure of the polycrystalline phase occurred in S2 and S3 samples, plane corresponding to diffraction peaks centered at $2\theta \sim 20.01^\circ$, 28.52° , 33.11° , 47.39° and 56.12° could be assigned to Miller indices (211), (222), (400), (440) and (622), respectively. The lattice constant is related with plane spacing for the cubic crystal is given by following equation:

$$\frac{1}{d^2} = \frac{(h^2+k^2+l^2)}{a^2} \quad (3.1)$$

where d is the plane spacing, hkl are Miller indices for a particular plane. With the help of equation 3.1, we have calculated lattice parameter 'a' for sample S2 and S3 which are having values 10.68 Å and 10.82 Å, respectively. The lattice constant calculated from the XRD results is slightly larger than that of pure Y_2O_3 powders (having $a = 10.56$ Å) and no peak of neodymium were detected. This indicates that neodymium was integrated into the crystal lattice of yttrium oxide [17]. With inspecting carefully, all diffraction peaks move to



higher angles with annealed samples, implying the increase of lattice constant. With increased annealing temperature, the deviation of the angle increased because of the larger atomic radius of Nd^{3+} ($R= 1.08 \text{ \AA}$) replacing the smaller atomic radius of Y^{3+} ($R= 0.89 \text{ \AA}$) in crystal cells, leading to a larger lattice constant [14]. However, the diffraction characteristics of Y_2O_3 crystalline phases were still observed in the XRD patterns of S3 sample. The average crystalline size for sample S2 and S3 has been calculated using well known Debye-Scherrer's equation which is given below:

$$D=K\lambda/\beta\text{Cos}(\theta) \quad (3.2)$$

where θ the Bragg angle of diffraction lines, λ is the wavelength of incident X-ray and β is the full width at half maximum (FWHM). The average size has been calculated as 10 and 21 nm, for sample S2 and S3 respectively. According to Scherrer formula, the peak will be narrow and sharp when the crystal size is bigger. Thus, this result can be attributed to growing of the crystal with rise of annealing temperature. We know that along heat treatment, dislocations become the main lattice defect, which decreases with increasing temperature. One may also estimate minimum dislocation density of the particular structure using the relation: $\rho \approx 1/\langle D \rangle^2$ [18-19]. The dislocation density of the samples S2 and S3 are found to be $\sim 8.26 \times 10^{14} \text{ m}^{-2}$ and $2.26 \times 10^{14} \text{ m}^{-2}$, respectively. One may also notice in as prepared and annealed samples that there is no appearance of silica neither in amorphous form nor as crystalline structure (quartz), which means that the presence of silica hardly change the structure of the host material. Therefore, we can say that SiO_2 is acting as a sintering agent in all the prepared samples. Moreover, atomic radius of Si is nearly half of the atomic radius of Y, and due to that diffraction intensity of silica was weakened and it is also shielded by the diffraction peaks of cubic Y_2O_3 .

3.3 Fourier Transform Infrared (FTIR) Spectroscopy

FTIR spectra of Nd^{3+} doped $\text{Y}_2\text{O}_3:\text{SiO}_2$ samples were taken at room temperature in the spectral range 400-4000 cm^{-1} . It exhibit different intensive sharp, intermediate and broad infrared absorption bands. FTIR spectrum of the sample S1 shown in the Fig. 3.3 having three strong broad-absorption bands centered around 3400 cm^{-1} , 1641 cm^{-1} and 1092 cm^{-1} .

Generally, in the FTIR spectra of silica, the absorption band around 3450 cm^{-1} and 3400 cm^{-1} are assigned to the stretching vibration of H-O-H and surface silanol group (Si-OH), respectively [19-20]. These vibrations overlap with each other and results in the broadening of the band. The absorption bands around 1641 cm^{-1} and 1101 cm^{-1} are due to bending of H-O-H absorbed at silica surface and asymmetric stretching of Si-O-Si, respectively [21]. The two medium size absorption bands around 803 cm^{-1} and 468 cm^{-1} are attributed to symmetric stretching and bending vibration of the Si-O-Si bond respectively, while the shoulder at 970 cm^{-1} could be assigned to Si-OH group [22]. Furthermore, FTIR spectrum of the sample S1 depicts few absorption peaks around 2360 cm^{-1} , 1483 cm^{-1} , 1359 cm^{-1} and 1315 cm^{-1} which could be due to organic/inorganic impurities like C=O, CO_3^{2-} and NO_3 [23].

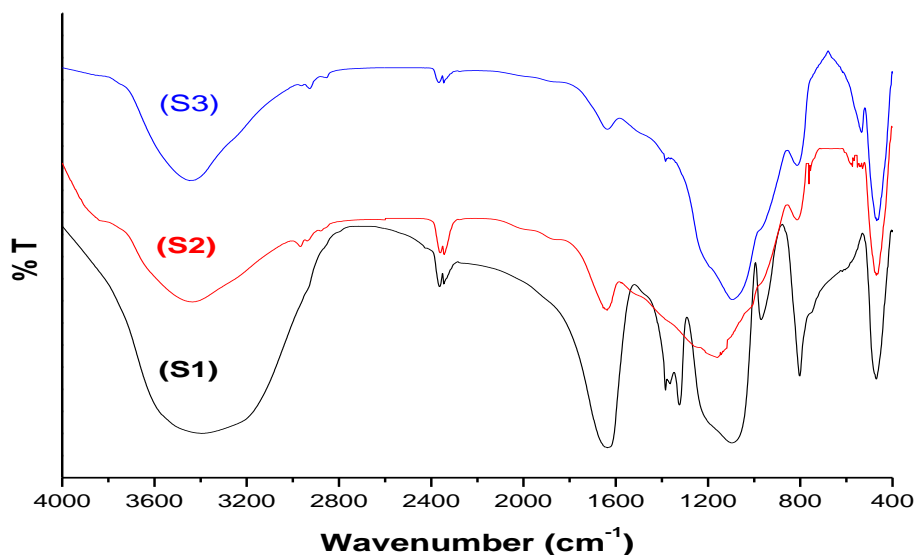


Figure 3.3: FTIR spectrum for sample S1, S2 and S3.

In the FTIR trace of the sample S2 annealed at temperature 450°C, one can notice a marginal decrease in broadening of strong- and medium- size absorption bands as shown in the Fig. 3.3. Spectrum of sample S2 contains no trace of organic impurities and there is also a significant decrease in absorption around 1640 cm⁻¹ which implies evaporation of organic impurities and absorbed water from the sample. Further, it can also be seen that a new absorption peak has been appeared around 562 cm⁻¹ attributed due to the stretching vibration of Y-O bond [5, 24]. But the noticeable feature of this FTIR trace is disappearance of N-O band which supports the XRD results of the corresponding sample. It is shown in the FTIR spectrum of sample S3 that high annealing temperature (850°C) completely eliminates pores, water molecules and volatiles matter which further confirms the densification of Nd³⁺ doped Y₂O₃:SiO₂ nanopowder. These features of the sample make the powder almost transparent for spatial frequency ranges 1650-3000 cm⁻¹.

In sample S3, the Y-O sharpness of absorption band increases with the increase in annealing temperature. This is obvious because of the fact that as size of nanocrystalline increases with temperature, the surface effects will be reduced. As a result of that, damping of surface mode absorption will decrease and Y-O absorption bands become narrowed. Moreover, the FTIR of samples S2 and S3 does not show any trace of absorption Si-O-Y/ Si-O-Nd phases. Therefore, FTIR studies of all samples confirm the presence of crystalline Y₂O₃ phase with silica and agreed with XRD results of the corresponding samples.

3.4 Transmission Electron Microscopy (TEM) Analysis

The TEM images of the as-prepared and annealed powder samples are shown in the Fig. 3.4. The samples were prepared for TEM imaging by drying the aforesaid samples on a copper grid that was coated with a thin layer of carbon and then analyzed. As expected, micrograph of the sample S1 in the Fig. 3.4 shows a typical chain-like structure of acidic gel of precursors with the diffusion of different nanoparticles. This stage indicated the start of reaction between precursors, yet, the crystalline phase was not appeared. The micrographs of as prepared

samples show asymmetric distribution of precursor concluded that TEM results are in close agreement with FTIR & XRD data.

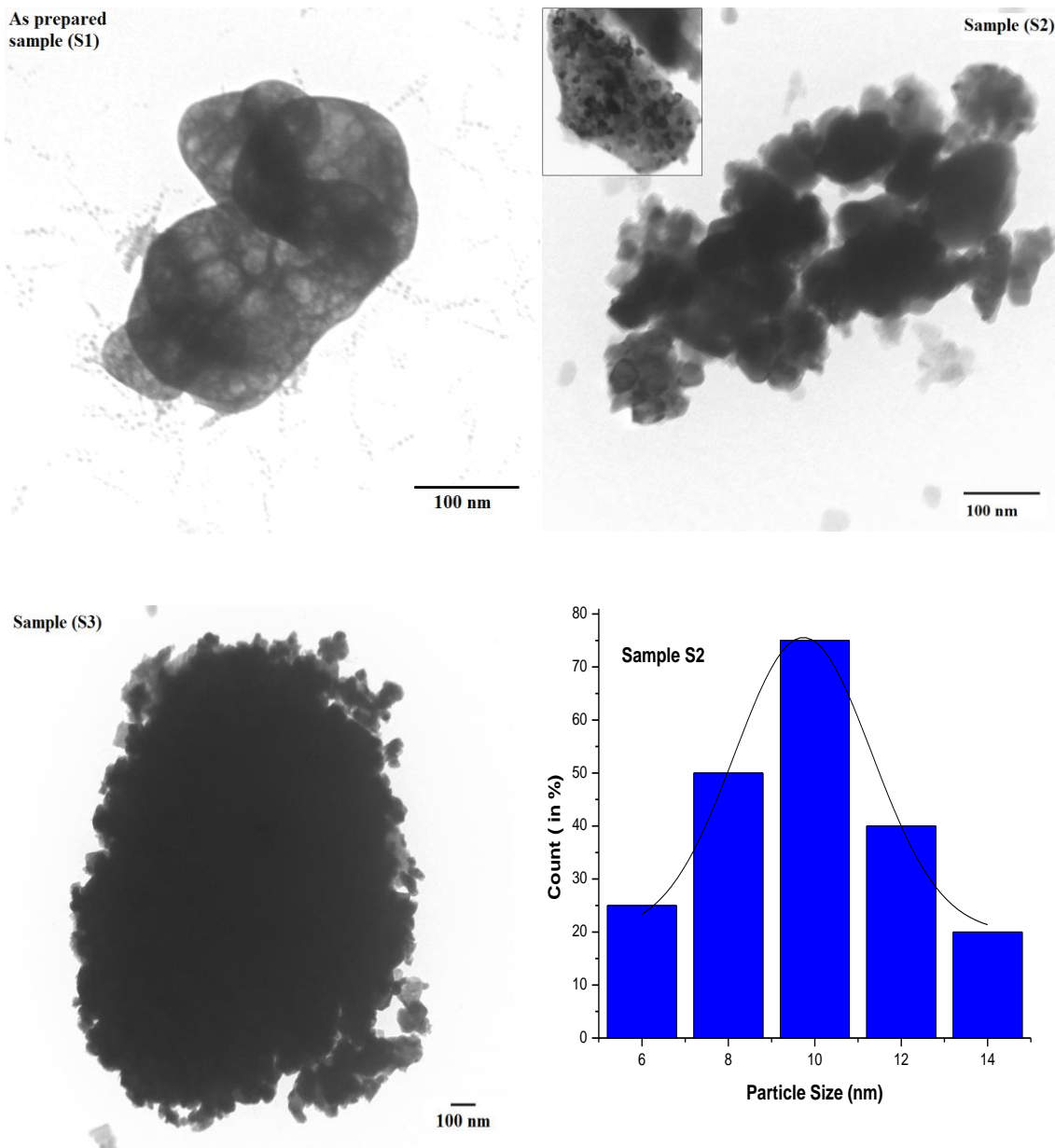


Figure 3.4: TEM micrograph of sample S1, S2, S3 and histogram for annealed sample S3.

A radical change in the structural morphology was found when heat treatment of the sample was implemented at around 450°C in sample S2. The TEM image of sample S2 shows quasi-spherical shape of yttria nanocrystallites which are somehow agglomerated. The inset of the micrograph of sample S2 shows some non agglomerated nanoparticles having average size ~11 nm. The particles size determined by TEM has also been compared with XRD analysis. There is a close agreement of particle sizes obtained by TEM with Debye Scherer results. However the particle size from the micrograph of samples S2 and S3 is found slightly greater than as obtained by XRD results. This discrepancy may be understood due to the intrinsic defects present and dislocations in the lattice of these samples [19].

The particle size distribution of sample S2 has been carried out by plotting with respective histogram as shown in the Fig. 3.4. The histogram represents a bar graph that illustrates frequency of occurrence versus the particle size range. It is clear from the Fig. 3.5 that some of the large particles are made up by agglomeration of small particles, which creates difficulty to determine the exact particle size. That's why we use the histograms for distribution of particle size which was found to be ~ 6-14 nm range for the sample S2. One may notice that 75 % of particles are having size ~10 nm. With the increase in annealing temperature, the crystallinity and densification is improved which is exhibited in the micrograph S3. Due to high agglomeration, histogram for sample S3 has not been plotted because nanocrystallites are not distinguishable.

IV. CONCLUSIONS

The present study demonstrates the versatility of the sol gel method to yield highly dense nanopowder of the neodymium doped in the composite of Y_2O_3 - SiO_2 binary oxide at a low annealing temperature (450 °C) when compared to the temperature (>1400–1600°C) required for the usual solid-state synthesis. The XRD analysis indicates that Nd^{3+} ion is perfectly integrated in to the crystal lattice of cubic yttrium oxide. The average sizes of the nanocrystallites were calculated from the diffraction line width based on the D–S formula, W–H plots and TEM histograms which is found ~ 10 & 21 nm for annealed samples S2 & S3, respectively. These types of ceramics material offers possibility of fabricating high optical quality Nd-doped Y_2O_3 - SiO_2 powder for solid state laser material, IR windows, lamp envelopes etc.

REFERENCES

- [1.] R.G. Haire and L. Eyring, Comparisons of the Binary Oxides, Handbook on the Physics and Chemistry of Rare Earths, North- Holland, Amsterdam, 18 (1994).
- [2.] N. C. R. Babu, C. S. Rao, M. G. Brik, G. N. Raju, I. V. Kityk and N. Veeraiah, Appl. Phys. B, 110 (2013) 335-344.
- [3.] X. Yu, Y. Shan, G. Li and K. Chen, J. Mater. Chem. 21 (2011) 8104-8109.
- [4.] L. Zhang, Z. Huang, and W. Pan, J. Am. Ceram. Soc., 98 (2015) 824–828.
- [5.] R. Ahlawat, Journal of Alloys and Compounds, 638 (2015) 356–363.
- [6.] S. Kochawattana, A. Stevenson, Sang-Ho Lee, M. Ramirez, V. Gopalan, J. Dumbb, V. K. Castillo, G. J. Quarles, G. L. Messing, Journal of the European Ceramic Society, 28 (2008) 1527–1534.
- [7.] M. Walsh, J. M. McMahon, W. C. Edwards, N. P. Barnes, R. W. Equall, R. L. Hutcheson, J. Opt. Soc. Am. B, 19 (2002) 2893-2903.
- [8.] G. Liu, G. Hong, H. Solid State Chem., 78 (2005) 1647-1651.
- [9.] A. Fukabori, V. Chani, J. Pejchal, K. Kamada, A. Yoshikawa, T. Ikegami, Optical Materials, 34 (2011) 452–456.
- [10.] Yu. I. Pazura, V. N. Baumer, T. G. Deyneka, O. M. Vovk, R. P. Yavetskiy, Functional Materials, 17 (2010) 107-113.
- [11.] W. H. Wong, K. K. Liu, K. S. Chan, and E. Y. B. Pun, J. Cryst. Growth, 288 (2006) 100-104.
- [12.] H. Liang, Z. Zheng, B. Chen, Q. Zhang, and H. Ming, Mater. Chem. Phys., 86 (2004) 430-4.
- [13.] A. Ikesue, T. Kinoshita, K. Kamata, J. Am. Ceram. Soc. 78 (1995) 1033-1040.



- [14.] X. Zhang, G. Fan, X. Wang, M. Fu, and W. Lu, *Ferroelectrics Lett. Sec.*, 43 (2016) 19-24.
- [15.] Rachna , P. Aghamkar, *Optical Materials*, 36 (2013) 337–341.
- [16.] B. D. Cullity, *Elements of X-ray Diffraction* (1959) Addition-Wesley U.S.A..
- [17.] S. Liu, Y. Sang, Y. Lv, H. Liu, *J Inorg Organomet Polym* (2011) DOI 10.1007/s10904-011-9510-x.
- [18.] R. Ahlawat, *Ceramics International*, 41 (2015) 7345-7351.
- [19.] P. Aghamkar, S. Duhan, M. Singh, N. Kshore and P. K. Sen, *J. Sol-Gel Sci Technol*, 46, (2008) 17-22.
- [20.] O. A. Graeve, S. Varma, G. Rojas-George, D. R. Brown and E. A. Lopez, *J. Am. Ceram. Soc.*, 89 (2006) 926-931.
- [21.] M. Yu, J. Lin and J. Fang, *J. Chem. Mater.*, 17 (2005) 1783-1791.
- [22.] X. L. Song, N. Jiang, Y. K. Li, D. Y. Xu, and G. Z. Qiu, *Mater. Chem. Physics*, 110 (2008) 128-135.
- [23.] Y. K. Kim, H. K. Kim and D. K. Kim, G. Cho, *J. Mater. Res.* 19 (2004) 413-416.
- [24.] P. A. Tanner and L. S. Fu, *Chem. Phys. Lett.*, 470 (2009) 75-79.
- [25.] R. Srinivasan, R. Yogamalar, A. C. Bose, *Materials Research Bulletin*, 45 (2010) 1165-1170.